Bilateral ANR/RSF collaboration - Franco-Russian project

NORMA

Efficient simulation of Noise Of Rotating Machines

ANR Project Number : ANR-19-CE40-0020-01
RSF Project Number : 20-41-09018 ANR

Deliverable T5-D1

Specification of test cases and first reference calculations (1): single rotor, (2): multirotor

Vladimir Bobkov, Tatiana Kozubskaya

Keldysh Institute of Applied Mathematics RAS, Moscow

August 2021

Abstract

The set of model problems related to the single-rotor and multi-rotor configurations simulation are formulated for the purpose of evaluating the developed particular methods and approaches, as well as demonstrating the effectiveness of the full computational algorithm built on their basis. Also the results of first calculations presented.

1 Task 5 model problems 1: single rotor systems

The model problems of the first category are leads to the task of modeling the system of the helicopter "rotor + fuselage". This category includes the following three subproblems.

1.1 Model problem 1.1: flow near single isolated rotor

The subproblem 1.1 (SP1.1) is problem of simulating the flow around a single isolated rotor and the noise generated by it in the hover mode in a non-inertial rotating frame of reference using hybrid RANS-LES scale-resolving methods. The goal of solving this problem is to compare the scale-resolving methods among partners in application to the simulation of turbulent flow and noise (including broadband noise) in the near and far field.

For the SP1.1 the problem of modeling the flow around the Caradonna-Tung rotor was chosen [1]. The problem was chosen due to the presence of a large amount of experimental data (Fig. 1). Including, for a wide range of velocities, the pressure distributions measured in the physical experiment in various sections of the blade, as well as the azimuthal evolution of the position of the tip vortex core.

The configuration of the propeller being modeled includes two rectangular blades built on the basis of the NACA-0012 airfoil without twist (Fig. 1). The blade angle is fixed at 8°. The rotor radius is 1.143 m, the blade chord is 0.1905 m. For the simulation, the axial flow mode was selected at a rotor speed of 650 RPM, which corresponds to the blade tip velocity of 77.8 m/s and the tip Mach number $M = 0.228$.

1.2 Model problem 1.2: external flow near single solid obstacle (helicopter fuselage)

The SP1.2 is problem of modelling the external flow around a single solid obstacle (helicopter fuselage) by the traditional method with a mesh aliged to the body surface (so-called "body-fitted" method) and a method of immersed boundary conditions (IBM). The goal of this subproblem is to compare two approaches to modeling the flow around solid bodies.

For the flow near rotor fuselage modelling problem the chosen well-known ROBIN (Rotor Body INterfere) fuselage (see Fig. 2) simulation case was chosen. It is noticeable, that the whole fuselage shape described analytically [2].

The fuselage length is $3.15m$, the flow velocity is $V_{flow} = 40\ m/s$ with zero incline angle. The Reynolds number calculated using the fuselage half-length ("rotor radius") and external flow velocity is $Re = 4 \times 10^6$.

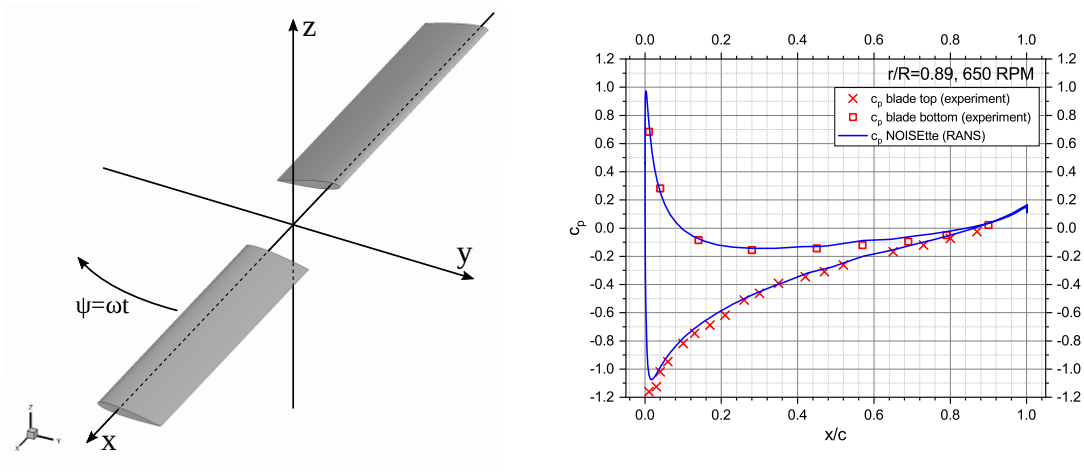

Figure 1: The Caradonna&Tung rotor geometry (left) and typical pressure coefficient distribution (right)

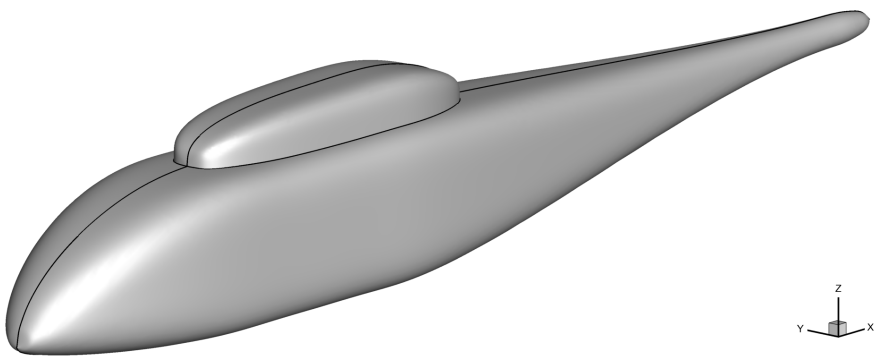

Figure 2: The ROBIN helicopter model fuselage

Besides the experimental data were is calculations results - for example [3] to compare with.

1.3 Model problem 1.3: "rotor + fuselage" system

The system of fuselage in presence of rotor can be modeled by combining the problem 1.1 and 1.2. In other words within the problem 1.3 is it proposed to model rotating Caradonna-Tung rotor near the ROBIN fuselage.

2 Task 5 model problems 2: multi-rotor systems

Model problems of the second category leads to the problem of modeling the "fuselage + system of rotors" system. It is implied that this is small-scaled UAV's rotor/systems. This category includes the following subtasks.

2.1 Model problem 2.1: isolated rotating rotor in hover

The SP2.1 is problem of simulating an isolated rotating rotor in hover using two methods: the traditional method is to simulate an external turbulent flow near a rotor using the Euler equations or a RANS approach on a mesh aligned with the rotor surface in a non-inertial rotating frame of reference and the method of immersed boundary conditions (IBM). The goal of this subproblem is to compare two approaches to modeling the tonal noise of a single rotor in a far field.

For this SP the small-scaled UAV rotor was chosen. In 2005 J. B. Brandt from University of Illinois, Urbana-Champaign(UIUC) Applied Aerodynamics Group within his PhD work [4] tested about 70 types of small scaled UAV rotors. Based on these results the open UAV rotors database was created [5, 6]. It includes rotors geometry description and experimental setup and results.

From this set of rotor models the most "moderate" one was choesn - APC Slow Flyer 10x4.7 UAV rotor (APC-SF). The APC-SF rotor (Fig. 3) is small-scaled UAV rotor with thin twisted blades and designed for rotational speed $2000 - 20000\ RPM$.

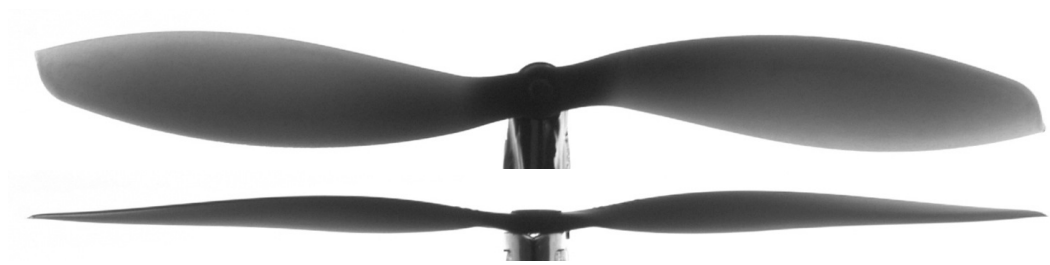

Figure 3: APC Slow Flyer 10x4.7 rotor (top and side view)

According to the manufacturer specs blade of the rotor based on the Eppler E63 airfoil (blade inner part) (2.1.1) and Clark-Y airfoil (2.1.2) (near blade tip).

In [4] work real chord and twist distributions along the blade were measured 2.1.3.

As per rotor specs: radius 127 mm, central body radius 12.7 mm and height 7.366 mm, mount hole diameter 6.35 mm.

2.1.1 Eppler E63 (E63 (4.25%) low Reynolds number airfoil

Eppler E63 low Reynolds number airfoil. Max thickness 4.3% at 22.8% chord, Max camber 5.3% at 50.5% chord (source)

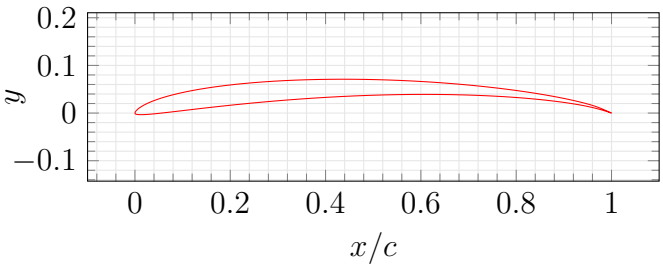

Figure 4: Eppler E63 airfoil

Table 1: Eppler E63 airfoil coordinates

x	y
100.000000	0.000000
99.719000	0.121000
98.938000	0.473000
97.751000	0.986000
96.173000	1.553000
94.164000	2.126000
91.717000	2.709000
88.861000	3.301000
85.624000	3.885000
82.039000	4.451000
78.141000	4.985000
73.968000	5.480000
69.562000	5.921000
64.967000	6.304000
60.229000	6.617000
55.394000	6.857000
50.509000	7.016000
45.624000	7.094000
40.786000	7.084000
36.043000	6.990000
31.441000	6.809000
27.026000	6.545000
22.840000	6.198000
18.920000	5.775000
15.304000	5.280000
12.023000	4.723000
9.103000	4.111000
6.568000	3.457000
4.435000	2.775000
2.714000	2.083000
1.416000	1.404000
0.536000	0.766000
0.076000	0.218000
0.055000	-0.141000
0.557000	-0.306000
1.651000	-0.330000
3.316000	-0.227000
5.550000	-0.004000
8.342000	0.315000
11.671000	0.708000
15.504000	1.151000
19.800000	1.620000
24.509000	2.093000
29.574000	2.546000
34.931000	2.962000
40.513000	3.319000
46.247000	3.605000
52.056000	3.803000
57.859000	3.907000
63.576000	3.907000
69.125000	3.806000
74.430000	3.604000
79.414000	3.310000
84.004000	2.930000
88.132000	2.482000
91.735000	1.979000
94.756000	1.439000
97.115000	0.887000
98.754000	0.410000
99.695000	0.102000
100.000000	0.000000

Table 2: Eppler E63 chamber line coordinates

x	y
0.076000	0.218000
0.536000	0.233451
1.416000	0.539578
2.714000	0.909380
4.435000	1.329850
6.568000	1.784656
9.103000	2.257919

x	y
12.023000	2.735841
15.304000	3.203942
18.920000	3.649465
22.840000	4.061678
27.026000	4.431557
31.441000	4.749991
36.043000	5.011559
40.786000	5.208308
45.624000	5.333963
50.509000	5.383135
55.394000	5.359911
60.229000	5.262000
64.967000	5.092841
69.562000	4.855180
73.968000	4.550796
78.141000	4.185046
82.039000	3.771840
85.624000	3.319593
88.861000	2.840614
91.717000	2.345256
94.164000	1.835410
96.173000	1.330213
97.751000	0.843952
98.938000	0.411387
99.719000	0.107487
100.000000	0.000000

2.1.2 CLARK Y airfoil

CLARK Y airfoil, Max thickness 11.7% at 28% chord, Max camber 3.4% at 42% chord (source)

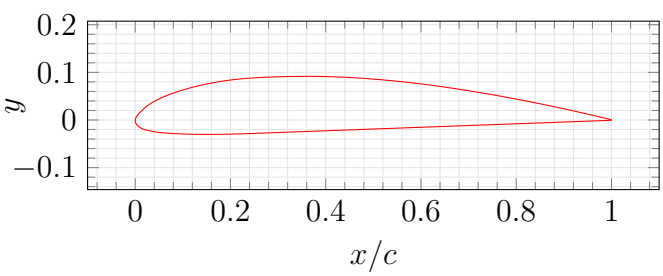

Figure 5: CLARK Y airfoil

Table 3: CLARK Y airfoil coordinates

x	y
100.000000	0.059930
99.000000	0.296900
98.000000	0.533350
97.000000	0.768680
96.000000	1.002320
94.000000	1.462390
92.000000	1.911560
90.000000	2.350250
88.000000	2.778910
86.000000	3.197400
84.000000	3.605360
82.000000	4.002450
80.000000	4.388360
78.000000	4.762810
76.000000	5.125650
74.000000	5.476750
72.000000	5.815990
70.000000	6.143290
68.000000	6.458430
66.000000	6.760460
64.000000	7.048220
62.000000	7.320550
60.000000	7.576330
58.000000	7.814510
56.000000	8.034800
54.000000	8.237120
52.000000	8.421450
50.000000	8.587720
48.000000	8.735720
46.000000	8.864270
44.000000	8.971750
42.000000	9.056570
40.000000	9.117120
38.000000	9.152120
36.000000	9.162660
34.000000	9.150790
32.000000	9.118570
30.000000	9.068040
28.000000	9.000160
26.000000	8.908400
24.000000	8.783080
22.000000	8.614330
20.000000	8.392020
18.000000	8.106870
16.000000	7.757070
14.000000	7.343600
12.000000	6.862040
10.000000	6.299810
8.000000	5.643080
6.000000	4.875710
5.000000	4.427530
4.000000	3.912830
3.000000	3.302150

x	y
2.000000	2.537350
1.200000	1.785810
0.800000	1.373500
0.400000	0.892380
0.200000	0.580250
0.100000	0.372710
0.050000	0.233900
0.000000	0.000000
0.050000	-0.467000
0.100000	-0.594180
0.200000	-0.781130
0.400000	-1.051260
0.800000	-1.428620
1.200000	-1.697330
2.000000	-2.027230
3.000000	-2.260560
4.000000	-2.452110
5.000000	-2.604520
6.000000	-2.712770
8.000000	-2.845950
10.000000	-2.937860
12.000000	-2.996330
14.000000	-3.024040
16.000000	-3.025460
18.000000	-3.004900
20.000000	-2.966560
22.000000	-2.914450
24.000000	-2.851810
26.000000	-2.781640
28.000000	-2.706960
30.000000	-2.630790
32.000000	-2.555650
34.000000	-2.481760
36.000000	-2.408700
38.000000	-2.336060
40.000000	-2.263410
42.000000	-2.190420
44.000000	-2.117080
46.000000	-2.043530
48.000000	-1.969860
50.000000	-1.896190
52.000000	-1.822620
54.000000	-1.749140
56.000000	-1.675720
58.000000	-1.602320
60.000000	-1.528930
62.000000	-1.455510
64.000000	-1.382070
66.000000	-1.308620
68.000000	-1.235150
70.000000	-1.161690
72.000000	-1.088230
74.000000	-1.014780
76.000000	-0.941330
78.000000	-0.867880
80.000000	-0.794430
82.000000	-0.720980
84.000000	-0.647530
86.000000	-0.574080
88.000000	-0.500630
90.000000	-0.427180
92.000000	-0.353730
94.000000	-0.280280
96.000000	-0.206830
97.000000	-0.170110
98.000000	-0.133390
99.000000	-0.096660
100.000000	-0.059930

Table 4: CLARK Y chamber line coordinates

x	y
0.000000	0.000000
0.050000	-0.116550
0.100000	-0.110735
0.200000	-0.100440
0.400000	-0.079440
0.800000	-0.027560
1.200000	0.044240
2.000000	0.255060
3.000000	0.520795
4.000000	0.730360
5.000000	0.911505
6.000000	1.081470
8.000000	1.398565
10.000000	1.680975
12.000000	1.932855
14.000000	2.159780
16.000000	2.365805
18.000000	2.550985
20.000000	2.712730
22.000000	2.849940
24.000000	2.965635
26.000000	3.063380
28.000000	3.146600
30.000000	3.218625
32.000000	3.281460
34.000000	3.334515
36.000000	3.376980
38.000000	3.408030

x	y
40.000000	3.426855
42.000000	3.433075
44.000000	3.427335
46.000000	3.410370
48.000000	3.382930
50.000000	3.345765
52.000000	3.299415
54.000000	3.243990
56.000000	3.179540
58.000000	3.106095
60.000000	3.023700
62.000000	2.932520
64.000000	2.833075
66.000000	2.725920
68.000000	2.611640
70.000000	2.490800
72.000000	2.363880
74.000000	2.230985
76.000000	2.092160
78.000000	1.947465
80.000000	1.796965
82.000000	1.640735
84.000000	1.478915
86.000000	1.311660
88.000000	1.139140
90.000000	0.961535
92.000000	0.778915
94.000000	0.591055
96.000000	0.397745
97.000000	0.299285
98.000000	0.199980
99.000000	0.100120
100.000000	0.000000

2.1.3 APC Slow Flyer 10x4.7 rotor blade geometry

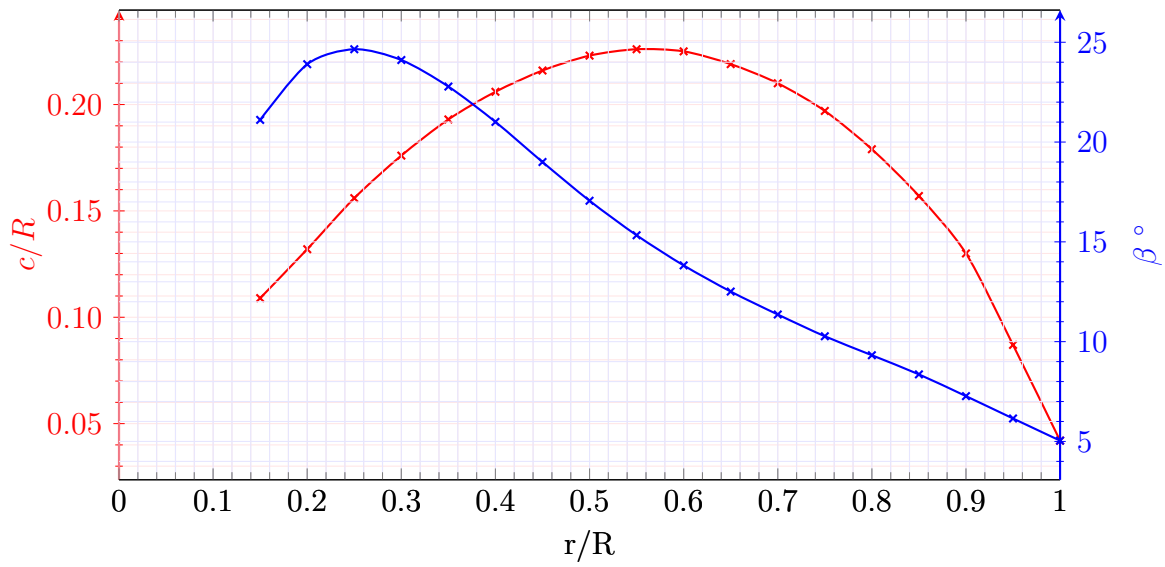

Figure 6: Blade twist and chord length distribution

Table 5: Blade twist and chord length

r/R	c/R	β °
0.15	0.109	21.11
0.20	0.132	23.90
0.25	0.156	24.65
0.30	0.176	24.11
0.35	0.193	22.78
0.40	0.206	21.01
0.45	0.216	19.00
0.50	0.223	17.06
0.55	0.226	15.33
0.60	0.225	13.82
0.65	0.219	12.51
0.70	0.210	11.36
0.75	0.197	10.27
0.80	0.179	9.32
0.85	0.157	8.36
0.90	0.130	7.27
0.95	0.087	6.15
1.00	0.042	5.04

2.1.4 APC Slow Flyer 10x4.7 rotor aerodynamics

Within the experiment rotor efficiency against rotor advance ratio J was studied:

$$J = \frac{V}{nD} \tag{1}$$

where n - rotational speed (rotations per second), V - vertical flow velocity (meters per second) and D - rotor diameter (meters).

The thrust coefficient c_t, power coefficient c_p and rotor efficiency η defined as

$$c_t = \frac{T}{\rho n^2 D^4} \tag{2}$$

$$c_p = \frac{P}{\rho n^3 D^5} \tag{3}$$

$$\eta = J\frac{c_t}{c_p} \tag{4}$$

where T - rotor thrust, $P = 2\pi nQ$ - rotor power and ρ - air density.

Table 6: Static thrust and power coefficients

RPM	c_t	c_p
2377	0.1059	0.0431
2676	0.1079	0.0437
2947	0.1079	0.0437
3234	0.1104	0.0444
3494	0.1117	0.0450
3762	0.1143	0.0460
4029	0.1158	0.0466
4319	0.1177	0.0474
4590	0.1200	0.0484
4880	0.1223	0.0494
5147	0.1237	0.0500
5417	0.1252	0.0508
5715	0.1263	0.0513
5960	0.1278	0.0520
6226	0.1286	0.0524
6528	0.1299	0.0531

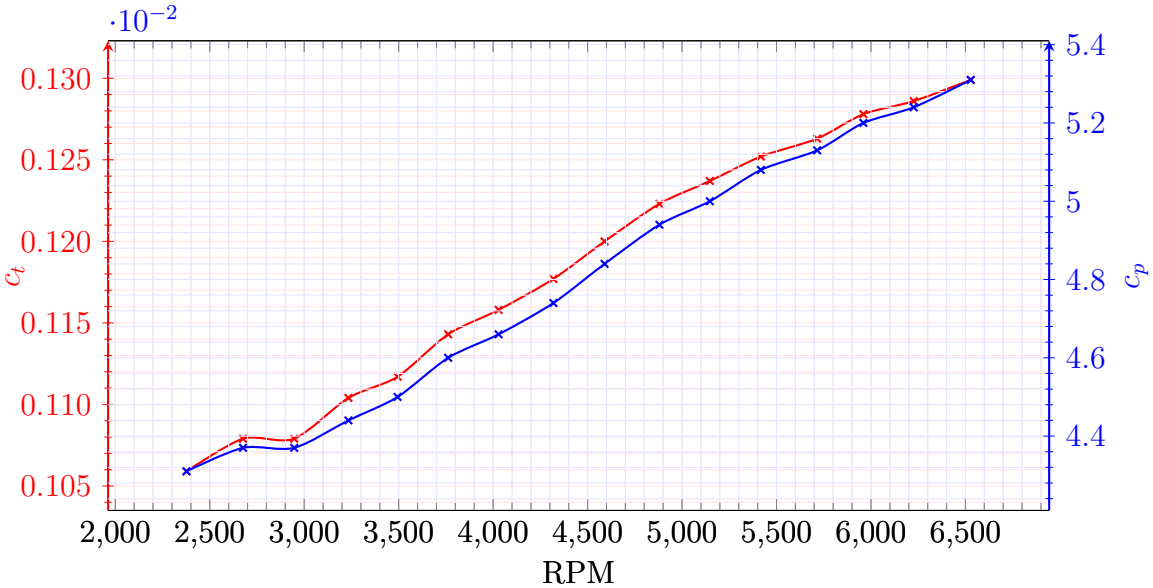

Figure 7: Static ($J = 0$) thrust and power coefficients against rotational speed

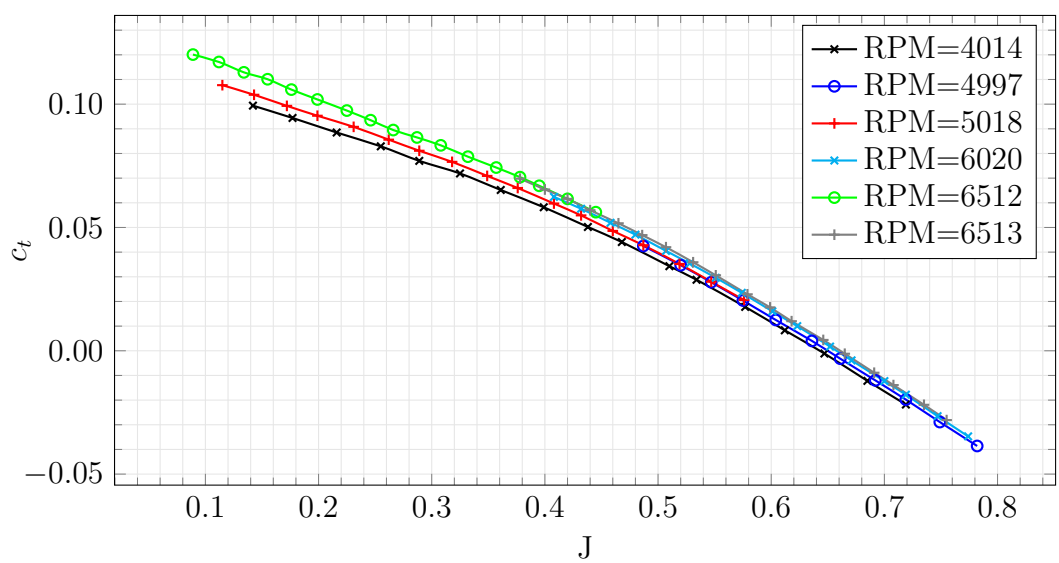

Figure 8: Thrust coefficient against advance ratio

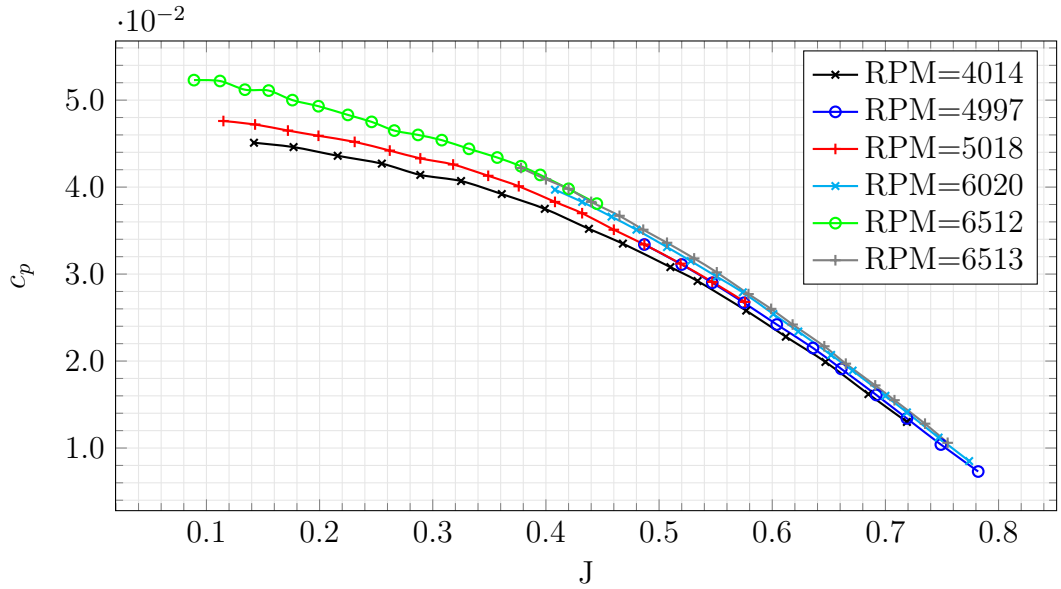

Figure 9: Power coefficient against advance ratio

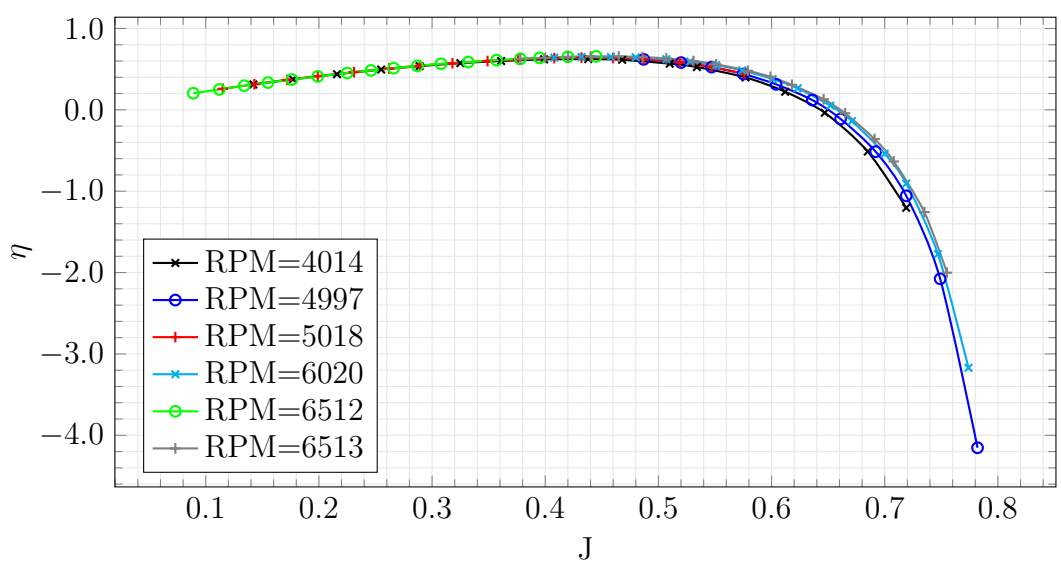

Figure 10: Rotor efficiency against advance ratio

Table 7: Thrust, power coefficients and efficiency against advance ratio

RPM	J	c_t	c_p	η
4014	0.142	0.0994	0.0451	0.312
	0.177	0.0944	0.0446	0.375
	0.216	0.0885	0.0436	0.438
	0.255	0.0829	0.0427	0.495
	0.289	0.0770	0.0414	0.537
	0.325	0.0719	0.0407	0.574
	0.361	0.0652	0.0392	0.600
	0.399	0.0582	0.0375	0.620
	0.438	0.0502	0.0352	0.624
	0.468	0.0441	0.0335	0.615
	0.510	0.0343	0.0308	0.567
	0.534	0.0288	0.0292	0.526
	0.577	0.0178	0.0258	0.398
	0.612	0.0083	0.0228	0.222
	0.647	-0.0011	0.0199	-0.036
	0.685	-0.0122	0.0162	-0.513
	0.719	-0.0218	0.0130	-1.204
4997	0.487	0.0425	0.0334	0.620
	0.520	0.0347	0.0311	0.581
	0.547	0.0278	0.029	0.525
	0.575	0.0204	0.0267	0.440
	0.604	0.0125	0.0242	0.313
	0.636	0.0040	0.0215	0.120
	0.661	-0.0032	0.0191	-0.112
	0.692	-0.0120	0.0161	-0.514
	0.719	-0.0198	0.0134	-1.057
	0.749	-0.0289	0.0104	-2.077
	0.782	-0.0386	0.0073	-4.153
5018	0.115	0.1077	0.0476	0.259
	0.143	0.1038	0.0472	0.314
	0.172	0.0993	0.0465	0.368
	0.199	0.0953	0.0459	0.414
	0.231	0.0908	0.0452	0.463
	0.262	0.0856	0.0442	0.508
	0.289	0.0811	0.0433	0.542
	0.318	0.0766	0.0426	0.573
	0.349	0.0709	0.0413	0.600
	0.376	0.0660	0.0401	0.620
	0.408	0.0597	0.0383	0.635
	0.432	0.0549	0.0370	0.641
	0.460	0.0486	0.0351	0.637
	0.487	0.0428	0.0334	0.623
	0.519	0.0352	0.0312	0.586
	0.547	0.0280	0.0291	0.528
	0.576	0.0206	0.0268	0.443
6020	0.408	0.0624	0.0397	0.641
	0.432	0.0576	0.0383	0.649
	0.458	0.0519	0.0366	0.650
	0.480	0.0471	0.0351	0.645
	0.507	0.0405	0.0331	0.622
	0.528	0.0354	0.0315	0.594
	0.551	0.0296	0.0297	0.549
	0.574	0.0235	0.0279	0.484
	0.601	0.0160	0.0254	0.378
	0.623	0.0100	0.0234	0.265
	0.652	0.0017	0.0207	0.052
	0.671	-0.0039	0.0189	-0.139
	0.700	-0.0123	0.016	-0.540
	0.719	-0.0178	0.0141	-0.906
	0.747	-0.0265	0.0112	-1.773
	0.774	-0.0347	0.0085	-3.171
6512	0.089	0.1201	0.0523	0.204
	0.112	0.1171	0.0522	0.250
	0.134	0.1129	0.0512	0.296
	0.155	0.1101	0.0511	0.335
	0.176	0.1059	0.0500	0.372
	0.199	0.1019	0.0493	0.410
	0.225	0.0974	0.0483	0.453
	0.246	0.0935	0.0475	0.484
	0.266	0.0895	0.0465	0.512
	0.287	0.0865	0.0460	0.540
	0.308	0.0833	0.0454	0.566
	0.332	0.0787	0.0444	0.587
	0.357	0.0743	0.0434	0.611
	0.378	0.0704	0.0424	0.627
	0.395	0.0669	0.0414	0.638
	0.420	0.0616	0.0398	0.651
	0.445	0.0562	0.0381	0.657
6513	0.378	0.0698	0.0422	0.625
	0.400	0.0654	0.0409	0.639
	0.420	0.0616	0.0398	0.650

RPM	J	c_t	c_p	η
	0.440	0.0570	0.0383	0.655
	0.465	0.0517	0.0367	0.656
	0.486	0.0469	0.0351	0.648
	0.507	0.0420	0.0336	0.632
	0.531	0.0359	0.0318	0.600
	0.551	0.0306	0.0302	0.560
	0.579	0.0229	0.0277	0.480
	0.599	0.0176	0.0260	0.406
	0.618	0.0120	0.0242	0.307
	0.646	0.0044	0.0217	0.130
	0.665	-0.0012	0.0197	-0.042
	0.691	-0.0089	0.0172	-0.359
	0.708	-0.0139	0.0155	-0.634
	0.735	-0.0219	0.0128	-1.257
	0.755	-0.0281	0.0106	-2.001

2.2 Model problem 2.2: system of 4 rotors

The SP2.2 is problem of simulating a system of 4 rotors using the method of immersed boundary conditions. The purpose of solving the model problem is to study the influence of the rotor's location on the total tonal noise when rotating rotors described using the IBM.

The rotor position and rotation directions corresponds to the typical quad-copter configuration (see Fig. 11).

2.3 Model problem 2.3: system of 4 rotors with fuselage

The SP2.3 is the problem of simulating the full system of 4 rotors and fuselage in hovering mode. In this case, the rotating rotors are modeled by IBM and the fuselage - using the traditional approach with a mesh aligned with the surface of a solid body. The goal of this problem is to study the noise in the far field of the system of 4 rotors and the fuselage, as well as to study the influence of the fuselage on the noise in the far field.

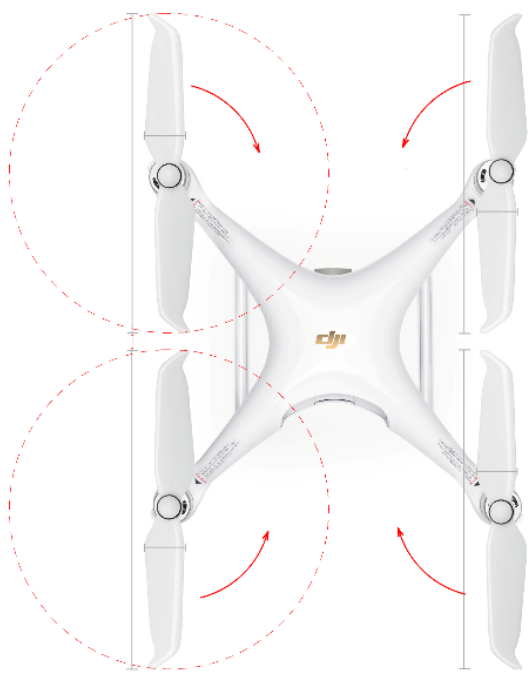

Figure 11: Quad-copter configuration

It is proposed to use the modern DJI quad-copter fuselage with four APC Slow Flyer 10x4.7 rotors described in 2.1 with proper rotation direction (see Fig. 11).

3 Model problem 1.1 (single helicopter rotor) simulation results

As mentioned in 1.1 the goal of the problem was to simulate flow and acoustics near Caradonna-Tung rotor using scale-resolving method.

The preliminary RANS calculation was performed to evaluate the developed flow downstream to the rotor. To do this the mixed-element unstructured mesh was build with $3.5M$ nodes. The performed calculation gives reasonable blade pressure distribution on the blade and flow-filed picture (see Fig. 1(right),Fig. 12 and Fig. 12).

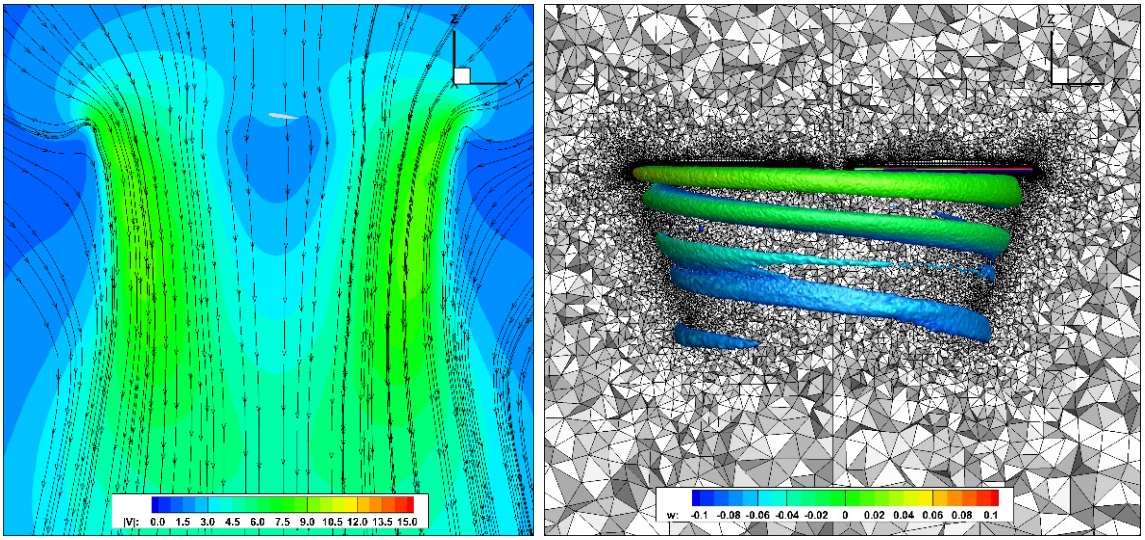

Figure 12: Caradonna-Tung RANS simulation results: velocity field in cross-section view (left) and mesh with Q-criterion iso-surface (right)

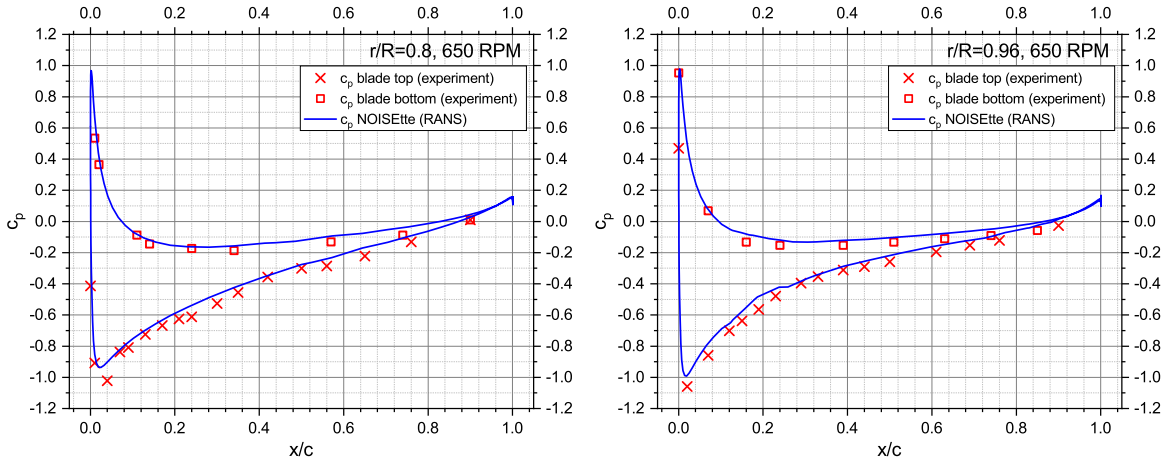

Figure 13: Caradonna-Tung RANS calculation: pressure coefficient distribution

For the IDDES flow simulation the mixed-element mesh was build. It included $92.5M$ nodes. The flow-field evaluated with RANS model was used as initial field. The turbulent structures captured with IDDES are mach more complicated than RANS - see Fig. 14. Due to big mesh size the data generation for the FWH analysis is not finished yet.

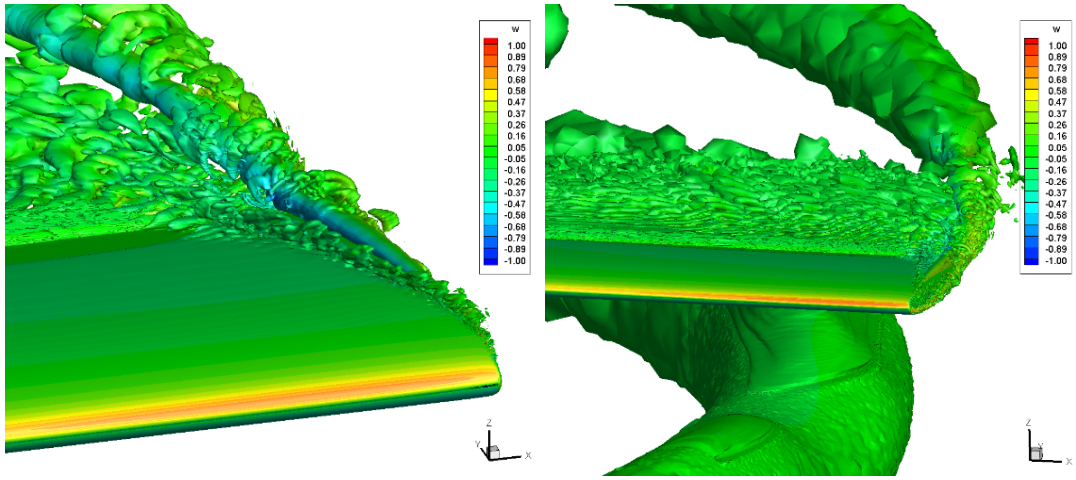

Figure 14: Caradonna-Tung IDDES simulation results: turbulent structures visualised with Q-criterion iso-surface

4 Model problem 1.2 (single helicopter fuselage) simulation results

As mentioned in 1.2 the goal of the problem was to simulate flow near the ROBIN fuselage using body-fitted and IBM methods.

Within this task the RANS-based simulation was performed. The mixed-element unstructured $1.6M$ nodes mesh was built for half of the fuselage (see Fig. 15).

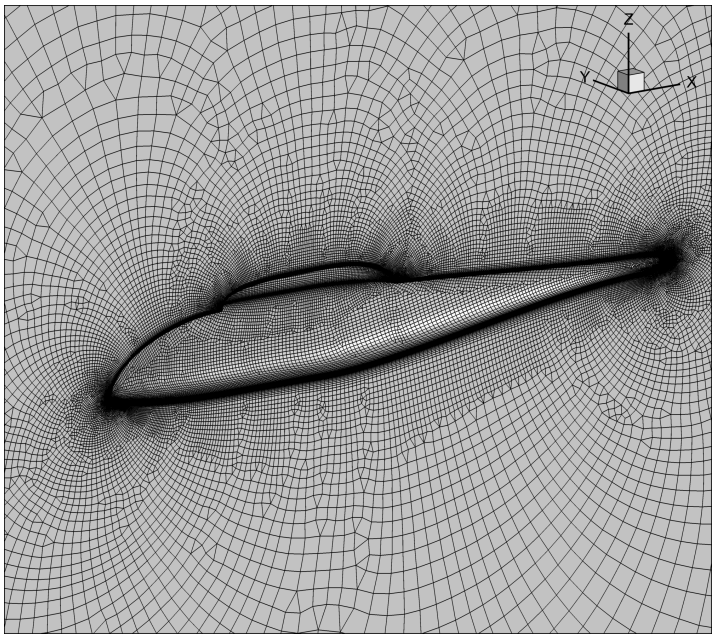

Figure 15: ROBIN fuselage body-fitted mesh for the RANS simulation

The flow and pressure distribution gathered in the RANS simulation are close enough to the experimental data and are well-aligned with other calculations - see Fig. 16.

The body-fitted results will be compared with ongoing IBM simulation.

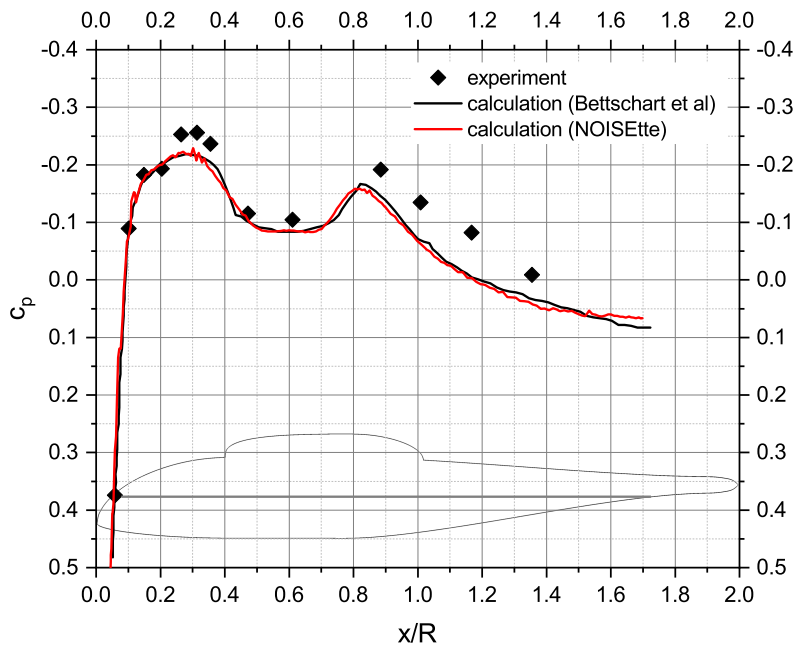

Figure 16: Pressure coefficient distribution along the fuselage $z = 0$ section

References

[1] F. X. Caradonna and C. Tung. Experimental and analytical studies of a model helicopter rotor in hover. Technical Report NASA-TM-81232, NASA, Ames Research Center, Moffett Field, California, September 1981.

[2] C. E. Freeman and R. E. Mineck. Fuselage surface pressure measurements of a helicopter wind-tunnel model with a 3.15-meter diameter single rotor. Technical Report NASA-TM-80051, NASA, NASA Langley Research Center Hampton, VA, March 1979.

[3] N. Bettschart, A. Desopper, R. Hanotel, and R. Larguier. Experimental and theoretical studies of helicopter rotor-fuselage interaction. In *Proc. of 18th Congress of the International Council of the Aeronautical Sciences*, number ICAS-92-4.8, 1992.

[4] J. B. Brandt. Small-scale propeller performance at low speed, 2005.

[5] J. B. Brandt and M.S. Selig. Small-scale propeller performance at low speeds – online database. https://m-selig.ae.illinois.edu/props/volume-1/propDB-volume-1.html, 2010.

[6] J. B. Brandt and M.S. Selig. Propeller performance data at low reynolds numbers. In *Proc. of 49th AIAA Aerospace Sciences Meeting*, number AIAA Paper 2011-1255, January 2011.